Boundary coupled dual-equation numerical simulation on mass transfer in the process of laser cladding

Yanlu Huang (黄延禄), Yongqiang Yang (杨永强), Guoqiang Wei (卫国强), Wenqing Shi (师文庆), and Yibin Li (李毅斌)

School of Mechanical Engineering, South China University of Technology, Guangzhou 510641

Received October 23, 2007

The coupled numerical simulation on fluid flow, heat transfer, and mass transfer in the process of laser cladding is undertaken on the basis of the continuum model. In the simulation of mass transfer in the laser molten pool, the concentration distribution in the regions on different sides of the interface between cladding layer and substrate is calculated separately and coupled at the co-boundary. The non-equilibrium solute partition coefficient is obtained from equilibrium solute partition coefficient according to the Sobolev model. By using the developed software which is based on the commercial software PHOENICS 1.4, the distribution of Fe in laser molten pool in an experiment of cladding Stellite 6 on 12CrMoV is calculated. The obtained results well coincide with the experimental ones.

OCIS codes: 140.0140, 140.3390, 000.3860.

Laser cladding is generally used to improve hardness, wear and corrosion resistance, and some other surface characteristics of individual products[1−4]. It is known that the mechanical properties for metal parts strongly depend on the parameters of crystalline structure, which depends on the alloy type, the cooling rate, and the alloy composition. For best performance, a low dilution for the cladding layer is expected. Generally, alloying should be uniform over the laser melted zone, while a grated distribution is demanded in some cases. Uniform alloying will be achieved, if the alloying additions are melted quickly as introduction into the pool and the combined convection diffusion of matter in the melt pool redistributes the solute effectively throughout the molten pool. Though insulation of solute would be expected to occur at the solidifying interface, high cooling rates, in combination with essentially uniform liquid composition at the solid-liquid interface, could greatly reduce the scale of local heterogeneity in composition.

Laser cladding is essentially a fusion and solidification process, which involves complicated interactions among the laser beam, metal powders, the substrate material, and processing gases. There are over ten variables which strongly influence the characteristics of the clad part[5]. Process optimization requires both theoretical and experimental understanding of the associated physical phenomena. Numerical modelling offers a cost-efficient way to better understand the related complex physics in a laser cladding process. It helps to reveal the effects and significance of each processing parameters on the desired characteristics of clad parts. Successful theoretical guidance enables intelligent closed-loop control in a high quality and stability process, and saves time and cost in transferring the laser cladding technology from one system to another. In the previous works, a model for the simulation of fluid flow, heat transfer, formation of the cladding layer, and interaction between laser beam and powder stream during the process of laser cladding with powder feeding has been presented, and it successfully predicted the characteristics of the laser cladding processing[5,6].

It has been pointed out that convection plays a major role in arc, laser, and electron beam weld pools[6−10]. Convection is the most important factor influencing the geometry of the pool including pool shape, undercut, and ripples, and can result in defects such as variable penetration, porosity, and lack of fusion. Convection is also primarily responsible for mixing and therefore affects the composition of the weld pool. Hence, some knowledge of the mechanisms and characteristics of material redistribution within the molten pool is desired to better understand the process of alloy production in laser cladding. The objectives of this work are to formulate a model for mass transport during laser cladding and evaluate the model predictions for different situations.

The mathematical model in this study is based on the following assumptions. 1) Laser beam profile is assumed to be Gaussian and constant along the z direction, i.e., the depth-of-focus effect is ignored. 2) The liquid metal is considered as an incompressible Newtonian fluid. Flow in the molten pool is considered to be laminar. 3) The fluid flow is driven by the buoyancy force in the molten pool and surface tension gradients on the molten pool surface. 4) The solid and liquid phases are considered as a continuum medium. The velocity of solid phase is zero. 5) There is no diffusion transport in solid phase.

The continuum model for binary solid-liquid phase change system[11] was used, and a fixed-grid and moving coordinate system was adopted to deal with fluid flow and heat transfer problem involving moving heat source. The governing equations in the moving frame can be written as follows.

The first one is the continuity equation

$$\frac{\partial(\rho)}{\partial t}+\frac{\partial(\rho u_j)}{\partial x_j}=0. \tag{1}$$

The second one is the momentum conservation equation

$$\frac{\partial(\rho u_i)}{\partial t}+\frac{\partial}{\partial x_j}(\rho u_i u_j)=\frac{\partial}{\partial x_j}(\mu\frac{\partial u_i}{\partial x_j})-\frac{\partial p}{\partial x_i}+S_i, \tag{2}$$

where ρ is the density, t is time, u_j is the average velocity in x_j direction: $u_j = f_{\rm l} u_{j\rm l}$, $f_{\rm l}$ is the liquid fraction, $u_{j\rm l}$ is the liquid velocity in x_j direction, μ is the viscosity coefficient, p is the pressure, and S_i is the source term. S_i is written as

$$S_i = -\frac{\mu}{K}\frac{\rho}{\rho_l}u_i + \frac{\partial}{\partial x_i}(\rho U_i u_i) + \rho_{\rm ref} g_i \beta (T - T_{\rm ref}), \quad (3)$$

where the first term is Darcy's term, representing the damping force when fluid passes through a porous medium (dendrite structures). K is osmotic coefficient which is defined by Carmon-Kozeny equation[12]:

$$K = K_0 \frac{f_{\rm l}^3}{(1 - f_{\rm l})^2}, \quad (4)$$

where K_0 is an empirical constant determined by the morphology of the porous medium. The second term in Eq. (3) is the additional convection term due to the sample movement and U_i is the sample velocity in x_i direction. The third term is the buoyancy due to temperature difference and T is the temperature, $T_{\rm ref}$ is the reference temperature, $\rho_{\rm ref}$ is the density at $T_{\rm ref}$, and g_i is the acceleration of gravity in x_i direction.

The third one is the energy conservation equation.

For a solid/liquid (S/L) binary phase system, the conservation of energy in enthalpy form can be written as

$$\frac{\partial(\rho h)}{\partial t} + \frac{\partial(\rho u_i h)}{\partial x_i} = \frac{\partial}{\partial x_i}(\frac{k}{c}\frac{\partial h}{\partial x_i}) + S_h, \quad (5)$$

where k is the mixture average conductivity, c is the mixture average specific heat, and S_h is the global source term,

$$S_h = q + \left[\frac{\partial}{\partial t}(\rho \Delta H) + \frac{\partial}{\partial x_i}(\rho u_i \Delta H)\right] + \frac{\partial}{\partial x}[\rho U_i (h + \Delta H)]. \quad (6)$$

In Eq. (6), the first term is the heat entering into the molten pool with powders, the second term is the transient and convection terms of the latent heat, and the third term is the heat transfer due to the sample movement including the sensible enthalpy term and latent heat one. ΔH is a function of temperature expressed as

$$\Delta H = \begin{cases} L & T \geq T_{\rm l} \\ L\phi_{\rm l} & T_{\rm s} < T < T_{\rm l} \\ 0 & T \leq T_{\rm s} \end{cases}, \quad (7)$$

where L is the latent heat, $T_{\rm s}$ and $T_{\rm l}$ are the solid and liquid temperatures, respectively.

The fourth equation is the solute conservation equation,

$$\frac{\partial}{\partial t}(\rho C) + \frac{\partial}{\partial x_j}(\rho u_j C) = \frac{\partial}{\partial x_j}(\rho D \frac{\partial C}{\partial x_j}) + S_{\rm c}, \quad (8)$$

where C is the mixture concentration,

$$C = f_{\rm s} C_{\rm s} + f_{\rm l} C_{\rm l}, \quad (9)$$

$C_{\rm s}$ and $C_{\rm l}$ are the concentrations in solid phase and liquid phase, respectively; D is the solute diffusion coefficient which can be written as

$$D = f_{\rm l} D_{\rm l} \quad (10)$$

with $D_{\rm l}$ being the molecular diffusion coefficient in liquid phase.

$S_{\rm c}$ in Eq. (8) is the derived source term when the solute conservation equation is written as the standard form, which can be defined as

$$S_{\rm c} = \frac{\partial}{\partial x_j}[\rho D \frac{\partial}{\partial x_j}(C_{\rm l} - C)] - \frac{\partial}{\partial x_j}[\rho u_j (C_{\rm l} - C)] - \frac{\partial(\rho U_j C)}{\partial x_j}, \quad (11)$$

where the first term is derived from the assumption (5), the second term is from the relative movement between the solid phase and the liquid phase, and the third term is from the relative movement of the laser beam and the workpiece. $C_{\rm l}$ can be calculated by

$$\frac{C_{\rm s}}{C_{\rm l}} = k_{\rm ne}, \quad (12)$$

$$f_{\rm s} C_{\rm s} + f_{\rm l} C_{\rm l} = C, \quad (13)$$

where $k_{\rm ne}$ is the non-equilibrium solute partition coefficient, which is calculated by the following model presented by Sobolev[13]:

$$k_{\rm ne} = \begin{cases} \frac{k_{\rm eq}(1-\beta^2)+\beta}{1-\beta^2+\beta}, & V < D_{\rm l}/\delta \\ 1, & V > D_{\rm l}/\delta \end{cases}, \quad (14)$$

where $k_{\rm eq}$ is the equilibrium solute partition coefficient, V is the interface moving speed, δ is the atomic layer space, β denotes the comparison of speed for the interface moving and the atom diffusion:

$$\beta = \frac{V\delta}{D_{\rm l}}. \quad (15)$$

The interface moving speed V can be obtained by

$$R = G \cdot V, \quad (16)$$

where R is the cooling rate and G is the normal temperature gradient at the interface.

The boundary conditions at the top surface include the energy gains, such as absorbed laser power, the heated powder entering the molten pool, and the energy losses such as convection and radiation heat transfers,

$$k\frac{\partial T}{\partial z} = \alpha \cdot I(x, y, z) - r_{\rm s}(T - T_{\rm s}) - \sigma \varepsilon_{\rm b}(T^4 - T_{\rm s}^4). \quad (17)$$

A Gaussian distribution was considered for the laser beam,

$$Q(r) = \frac{3P}{\pi R^2} \exp(\frac{-3r^2}{R^2}). \quad (18)$$

The thermocapillary force acts in the tangential direction of the free surface and is caused by the surface temperature gradient, and the relationship between them is

$$\mu\frac{\partial v}{\partial l_{\rm n}} = -\frac{\partial \gamma}{\partial T}\frac{\partial T}{\partial l_{\rm t}}. \quad (19)$$

In Eqs. (17) – (19), P is the laser power, T is temperature, Q is the initial laser intensity, r is the distance from a site in the laser spot to the center of the laser spot, α is the laser absorption, I is the laser intensity at the surface of the workpiece, T_s is the room temperature, r_s is the heat exchange coefficient, σ is the Stefan-Boltmann constant, ε_b is the emissivity, γ is the surface tension, v is the tangential velocity at the free surface, l_n and l_t denote the normal and tangential lengths, respectively.

The experimental case in this paper is cladding the satellite 6 alloy on 12CrMoV. The compositions of the alloys are listed in Tables 1 and 2. In the process of laser cladding, the solute is always different in the regions on both sides of the interface between the cladding layer and the substrate. In this study, Fe is the main solute in the cladding layer, while Co, Cr, W, and Ni are in the substrate. There are several kinds of metal solute in the substrate, but we can regard them as one, written as "Me", for their approximately equal diffusion coefficient in liquid metal[14].

The solute diffusion had opposite direction in the two regions, so the concentration distribution in the two regions on both sides of the interface was calculated separately and coupled at the co-boundary. Figure 1 is the schematic diagram of this model, in which P_{Fe} denotes the cell on the side of cladding layer and its boundary condition is B_{Fe} and P_{Me} denotes the cell on the side of substrate and its boundary condition is B_{Me}. The calculation can be implemented by the following procedure.

1) At beginning, C_{Fe} is assumed to be the initial Fe content of 12CrMoV and C_{Me} the initial Me content of satellite 6. And let $B_{Fe} = 1 - C_{Me}$, $B_{Me} = 1 - C_{Fe}$.

2) Solve the mass transfer equation at both sides of the interface, and then get the updated concentrations C_{Fe} and C_{Me}.

Table 1. Composition of 12CrMoV Steel (wt.-%)

C	Si	Mn
$1.45 - 1.70$	$0.25 - 0.40$	$0.20 - 0.35$
Cr	Mo	Fe
$11.0 - 12.50$	$0.40 - 0.60$	Bal.
V	S	P
$0.15 - 0.3$	≤ 0.025	≤ 0.025

Table 2. Composition of Satellite 6 Alloy (wt.-%)

C	Cr	Si	W	Fe	Mo	Ni	Co	Mn
1.15	29	1.1	4	3	1	3	Bal.	0.5

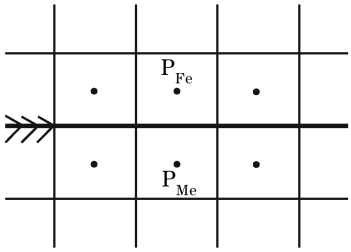

Fig. 1. Schematic diagram of the coupled boundaries between the two computed zones.

3) Update the boundary conditions: $B_{Fe} = 1 - C_{Me}$, $B_{Me} = 1 - C_{Fe}$.

4) Return to step 2), and repeat the computation.

Since continuum model had been adopted, explicit tracking of internal boundaries among solid, liquid and mushy regions were unnecessary, so fixed grid system was used in the numerical scheme. The governing equations were discretized using the control-volume-based finite-difference approach, with an upwind scheme for the convective terms. The SIMPLEST algorithm was adopted to resolve the velocity-pressure coupling in the momentum equations. Iteration solution was adopted to account for the coupling among the various equations. At each time-step, the velocity field was computed first by using the previously computed liquid fraction, permeability, and physical parameters. Then, the temperature and concentration fields were calculated. Next, the liquid fraction was updated based on the computed temperature, and the permeability and the physical parameters were updated according to the liquid fraction. The above computing procedure was repeated until convergent solutions were obtained.

The model is implemented by appending several self-developed modules to the commercial software PHOENICS 1.4. In order to accurately calculate the strong fluid flow and the mass transfer, the grid size at the laser irradiated area have to be adequately small. It is assumed that the domain is symmetrical in the y direction, therefore only half of the domain is considered. In this study, the overall computational domain size is $6 \times 4 \times 4$ (mm), corresponding to a uniform grid system of $90 \times 60 \times 60$. The boundary of the computational domain is considered far enough from the melt pool region so that infinite boundary conditions are employed. The time step is 0.0005 s. The properties of the materials are listed in Table 3.

The experiment was conducted by cladding satellite 6 on 12CrMoV steel with CO_2 laser. In the experiment, the laser power was 2800 W, the laser spot radius was 1.5 mm, the scanning speed was 10 mm/s, and the powder feeding rate was 0.41 g/s. To compare with the experimental results, the concentration at eight different sites in the sample was measured. The selected sites are sketched in Fig. 2 and their coordinates are listed in Table 4. The composite content was measured with electron probe microanalysis (EPMA-1600). Each site was measured for three times and their average values were approved.

Figure 3 shows the comparison of the numerical results and experimental results for the Fe content at the selected sites $1 - 5$ in the symmetric plane. It can be seen that the Fe content decreases with increasing the distance to the interface in the cladding layer. The Fe

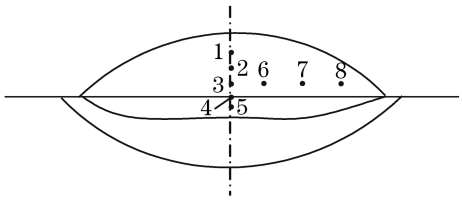

Fig. 2. Schematic diagram of the sites (numbered $1 - 8$) analyzed for composition in melting pool.

Table 3. Materials Properties

Properties	Satellite 6	12CrMoV
Density (kg/m^3)	8400	7800
Solid Thermal Conductivity (W/(m·°C))	$13.39 + 0.028T$	$65.0 - 0.05T + 2 \times 10^5 T^2$
Liquid Thermal Conductivity (W/(m·°C))	48.8	35
Specific Heat (J/(kg·°C))	416.7	610
Latent Heat of Fusion (J/kg)	3.1×10^5	2.47×10^5
Viscosity (m^2/s)	7.1×10^{-7}	7.6×10^{-7}
Melting Temperature (°C)	1354	1530
Eutectic Temperature (°C)	1265	1493
Thermal Expansion Coefficient	1.33×10^{-4}	1.33×10^{-4}
Surface Absorptivity	0.31	0.35
Surface Tension Coefficient	-1.12×10^{-4}	-1.25×10^{-4}

Table 4. Coordinates of the Measured Sites (μm)

Site	1	2	3	4
Coordinate	(0, 600)	(0, 400)	(0, 200)	(0, 0)
Site	5	6	7	8
Coordinate	(0, −100)	(400, 200)	(800, 200)	(1200, 200)

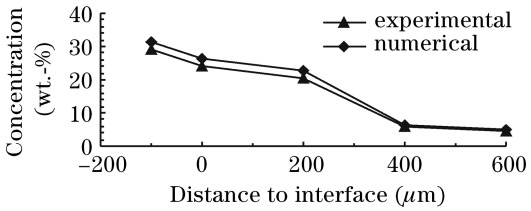

Fig. 3. Concentration distribution of Fe along the vertical direction in the longitudinal section of the melting pool.

content at site 5 in the substrate is much lower than the initial Fe content of 12CrMoV, which is due to the mixing of the cladding contents in the substrate. The numerical results coincide with the experimental ones basically.

Figure 4 is the comparison of the numerical results and experimental ones for Fe content in the cross section of the sample along y direction. It is obvious that the Fe content is approximately uniform at a specified height in the cladding layer. In despite of the acceptable differences between the numerical results and the experimental ones, the simulation successfully predicts the characteristic of the solute concentration distribution.

In the published researches, some found that the solute concentration was uniform in the whole molten pool[7−9], which also provided the foundation of the method for calculating the dilution of the cladding. It is understandable for the situations of low powder feeding rate. When the powder feeding rate was high, the convection eddy would be more complicated and lead to a gradient distribution of the substrate composite in the whole cladding layer.

In this paper, such a case in which the same technique parameters except for a low powder feeding rate were adopted was contrastively simulated. In this contrastive experiment, the diminished powder feeding rate was 0.22 g/s. Figure 5 shows the comparison of the numerical results and experimental ones for the Fe contents

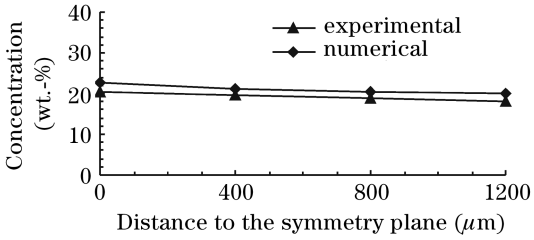

Fig. 4. Concentration distribution of Fe along the horizontal direction in the transverse section of the melting pool.

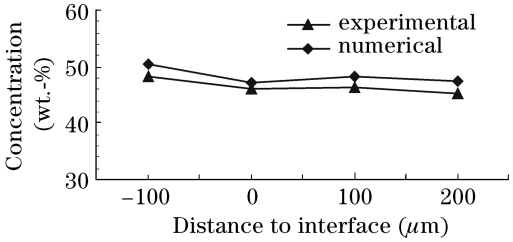

Fig. 5. Concentration distribution of Fe along the vertical direction in the longitudinal section of the melting pool for the contrastive experiment.

at different sites in the symmetric plane. It can be seen that the Fe content almost keeps constant with increasing the distance to the interface in the cladding layer. It is also shown in Fig. 5 that the Fe content is much higher than that in the previous experiment, because there is a higher dilution due to the lower powder feeding rate in the contrastive experiment.

In conclusion, a self-consistent three-dimensional (3D) model has been developed for a laser cladding process, which simulates heat transfer, phase changes, fluid flow, and mass transfer in the molten pool. Transport equations are solved with a controlled-volume finite difference method. Temperature, fluid velocity, and solute concentration are solved in a coupled manner. The method of separately calculating the concentration in the two regions on both sides of the interface between the cladding and the substrate can predict the solute concentration distribution in the laser molten pool. The nonequilibrium solute partition due to the rapid melting and solidification in laser cladding should be considered in the computation. A gradient solute concentration distri-

bution can emerge under some certain conditions, which may exploit a new way to produce graded coatings by using the laser cladding with powder feeding.

This work was supported by the National Natural Science Foundation of China under Grant No. 59871038 and the Foundation of State Key Laboratory of Laser Technology, Huazhong University of Science and Technology. Y. Huang's e-mail address is yanlu@scut.edu.cn.

References

1. J. Mazumder, J. Choi, K. Nagarathnam, J. Koch, and D. Hetzner, J. Miner. Met. Mater. Soc. (JOM) **49,** (5) 55 (1997).
2. H. Shao, X. Jiang, L. Wang, and Y. Hua, Chin. Opt. Lett. **4,** 589 (2006).
3. Y. Huang, N. Ma, D. Zou, G. Liang, and J. Su, Rare Metal Materials and Engineering (in Chinese) **32,** 999 (2003).
4. L. Pawlowski, Journal of Thermal Spray Technology **8,** 279 (1999).
5. Y.-L. Huang, G.-Y. Liang, J.-Y. Su, and J.-G. Li, Model. Simulat. Mater. Sci. Eng. **13,** 47 (2005).
6. Y. Huang, G. Liang, and J. Su, J. Univ. Sci. Technol. Beijing Miner. Metall. Mater. **11,** 13 (2004).
7. C. Chan, J. Mazumder, and M. M. Chen, Metall Trans A **15,** 2175 (1984).
8. X. Yang, T. Zheng, N. Zhang, M. Zhong, Y. Lin, and S. Gao, Acta Metall. Sin. B **5,** 315 (1992).
9. T. Chande and J. Mazumder, Appl. Phys. Lett. **41,** 42 (1982).
10. T. Chande and J. Mazumder, J. Appl. Phys. **57,** 2226 (1985).
11. W. D. Bennon and F. P. Incorpera, Int. J. Heat Mass Transfer **30,** 2161 (1987).
12. S. Asai and I. Muchi, Trans. Iron Steel Inst. Jpn. Int. **18,** 90 (1978).
13. S. L. Sobolev, Phys. Lett. A **199,** 383 (1995).
14. Thermo-Calc Software AB, *DICTRA Mobility Database Description Form* (2001).